Far-from-equilibrium universality in two-dimensional Heisenberg antiferromagnets

Zhaoyi Li,[1] Paolo Glorioso,[1] and Joaquin F. Rodriguez-Nieva[1,2]
[1]*Department of Physics, Stanford University, Stanford, California 94305, USA*
[2]*Department of Physics & Astronomy, Texas A&M University, College Station, Texas 77843, USA*

(Received 22 December 2022; accepted 12 September 2023; published 10 October 2023)

We study the far-from-equilibrium dynamics of isolated two-dimensional Heisenberg antiferromagnets. We consider spin-spiral initial conditions which imprint a position-dependent staggered magnetization (or Neel order) in the two-dimensional lattice. Remarkably, we find a long-lived prethermal regime characterized by self-similar behavior of staggered magnetization fluctuations, although the system has no long-range order at finite energy and the staggered magnetization does not couple to conserved charges. By exploiting the separation of length scales introduced by the initial conditions, we derive an analytical model that allows us to compute the spatial-temporal scaling exponents and power-law distribution of the staggered magnetization fluctuations, and find excellent agreement with numerical simulations using phase-space methods. The scaling exponents are insensitive to details of the initial condition, in particular, no fine tuning of energy is required to trigger the self-similar scaling regime. Compared with recent results on far-from-equilibrium universality on the Heisenberg ferromagnet, we find quantitatively distinct spatial-temporal scaling exponents, therefore suggesting that the Heisenberg model can host different universal regimes depending on the initial conditions. Our predictions are relevant to ultracold-atom simulators of Heisenberg magnets and driven antiferromagnetic insulators.

DOI: 10.1103/PhysRevB.108.144303

I. INTRODUCTION

Many-body systems out of thermodynamic equilibrium can exhibit universal phenomena beyond conventional equilibrium paradigms. Prominent examples include turbulence [1–3], aging [4], coarsening [5], surface growth [6], breakdown of transport [7], and percolation [8]. One common theme in the study of equilibrium and out-of-equilibrium universality is the emergence of self-similar behavior: microscopically distinct models can be classified into universality classes sharing the same scaling exponents. Unlike systems at thermodynamic equilibrium, far-from-equilibrium systems break a symmetry associated to detailed balance [9–11] and can therefore exhibit richer behaviors than their equilibrium counterparts. Such rich behaviors have been observed in driven-dissipative systems [12–16] where an external drive pushes the system to a nonthermal steady state while dissipation maintains energy balance, and in quenches of isolated systems where the system acts as its own bath [17–30]. These universal nonequilibrium regimes are now routinely probed in cold-atom experiments [31–35].

Conserved charges and order parameters, both of which are determined by symmetries and dimensionality of the system, play an important role in determining the nature of the scaling behavior. In some cases, nonconventional scaling behavior arises from the nonlinear dynamics of conserved charges in phase space. Examples include turbulent phenomena in fluids and nonthermal fixed points of bosonic theories where the self-similar scaling is governed by the *cascade* of conserved charges in momentum space [2,26–29], one-dimensional integrable systems where Kardar-Parisi-Zhang (KPZ) scaling arises due to the extensive number of conserved charges [36–39], and thermalizing systems in low dimensions which display a breakdown of local hydrodynamics [7,40,41] (see Ref. [42] for an example in kinematically constrained systems). In other cases, nonconventional scaling is induced by the dynamics of the order parameter. Examples include coarsening dynamics where self-similar scaling arises due to the growth of ordered domains [5,43,44], or aging dynamics where self-similar scaling arises due to quasi-long-range correlations close to criticality [30,45–47]. In general, quantities which are neither conserved nor couple with an order parameter are expected to relax in microscopic times and exhibit featureless dynamics.

Here we study the prethermal dynamics of isolated Heisenberg antiferromagnets and show that quantities which are neither conserved nor exhibit ordering at finite temperature can still exhibit slow relaxation and universal prethermal dynamics when initialized from certain excited states. In particular, using spin-spiral excited states with inhomogeneous Neel order (see Fig. 1), we find that large and slowly relaxing staggered magnetization fluctuations persist during a long-lived prethermal regime although the system exhibits no symmetry-breaking phase transition at finite temperature. In this prethermal regime, the staggered magnetization rapidly relaxes to zero but staggered magnetization fluctuations exhibit universal scaling governed by

$$C_{\boldsymbol{k}}(t) = \langle M_{-\boldsymbol{k}}(t) M_{\boldsymbol{k}}(t)\rangle = t^{\alpha} f(t^{\beta}|\boldsymbol{k}|), \tag{1}$$

with $\beta \approx 0.5$ and $\alpha \approx 1$. In Eq. (1), the universal function f also exhibits scaling $f(x) \sim 1/|x|^{\nu}$ for a broad range of momenta, with $\nu \approx 2.3$, and takes $O(1)$ values at the lowest momenta. The scaling exponents (α, β, ν) are universal in the sense that they are insensitive to details of the Hamiltonian or the initial condition. In particular, we emphasize that no fine tuning of energy is needed. Using a

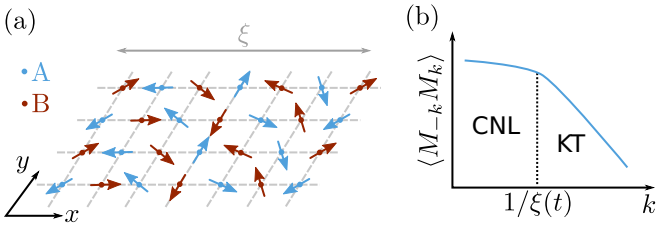

FIG. 1. (a) Schematics of the staggered spin-spiral initial state [see Eq. (3)]. The wave vector $\boldsymbol{q} = (q_x, 0)$ of the initial condition imprints a length scale $\xi(0) = 2\pi/q_x$ in the system at time $t = 0$. (b) We compute the scaling behavior of $\xi(t) \sim t^{\beta}$ using a continuous nonlinear (CNL) theory describing staggered magnetization fluctuations at small wave vectors $k \lesssim 1/\xi$, and we compute the power-law distribution $\langle M_{-k} M_k \rangle \sim 1/k^{\nu}$ of the function f in Eq. (1) using a kinetic theory (KT) of magnons valid for wave vectors $1/\xi \lesssim k \ll 1/\ell$.

continuous nonlinear model describing long-wavelength spin modes combined with a kinetic theory of interacting quasiparticles at shorter wavelengths, we are able to derive analytically the three scaling exponents (α, β, ν). These analytic values are shown to agree remarkably well with numerical simulations using phase-space methods.

We find that the origin of the prethermal scaling is related to the existence of spin modes whose gapless nature is protected by the global SU(2) symmetry. We show this by computing the unequal-time spin-spin correlation function [48], which exhibits linearly dispersing gapless modes even though the prethermal state is an intermediate-energy state far from the staggered ground state. A central insight in understanding the prethermal scaling in two-dimensional systems with SU(2) symmetry was discussed in recent works by one of us in the context of Heisenberg ferromagnets [49,50]. In the ferromagnetic case, the two-dimensional nature of the system bestows magnetization fluctuations a quasi-long-range character. In addition, the combination of magnetization being a conserved quantity and the constrained interactions resulting from the SU(2) symmetry gives rise to a universality class distinct from previously studied instances of scaling. Similarly to the ferromagnetic case, the two-dimensional nature of the antiferromagnet leads to quasi-long-range fluctuations of the staggered magnetization. However, unlike the ferromagnet, the staggered magnetization is not a conserved quantity. In spite of its nonconserved nature, we still find a parametrically long time window (controlled by nonuniversal parameters that depend on Hamiltonian details and the initial conditions) in which the system exhibits universal prethermal scaling.

We find that the Heisenberg antiferromagnet belongs to a different nonequilibrium universality class than previously studied models with similar features. Compared to the Heisenberg ferromagnet [50], we find clearly distinct scaling exponents, indicating that the same Hamiltonian with ferromagnetic and antiferromagnetic initial conditions lead to quantitatively distinct universal dynamics. We attribute such differences to the dispersion of emergent gapless modes and the effective interactions between them (see Sec. III). We also emphasize that the scaling regime discussed in this work is intrinsically different from the predictions of model G in the Halperin-Hohenberg classification [51]: while the latter describes universal behavior close to thermodynamic equilibrium, here we consider a dynamical regime where equilibrium properties, such as the fluctuation-dissipation relation, are violated. In comparison with O(n) theories in $d = 2$, we note that these models also exhibit linearly dispersing quasiparticles and long-range order at $T = 0$ [52]. We find that both O(n) theories and Heisenberg antiferromagnets exhibit similar (within numerical uncertainty) nonequilibrium spatial-temporal scaling exponents $\beta \approx 0.5$ and $\alpha \approx 1$, but they have clearly distinct values of the universal scaling exponent ν. The same conclusion applies when comparing nonrelativistic bosonic theories and antiferromagnets [we note that relativistic O(n) theories and nonrelativistic U(1) theories were shown to exhibit the same $\alpha = d\beta$ and $\beta \approx \frac{1}{2}$ exponents [53]]. We find that a different exponent ν arises because interactions between spin modes are soft due to the global SU(2) symmetry, whereas interactions between bosonic modes are hard-core in O(n) and U(n) theories.

Our predictions are relevant in a variety of experimental scenarios, both in condensed-matter and cold-atomic platforms. First, in recent years there have been remarkable advances in our experimental capabilities to probe the dynamics of isolated spin systems in low dimensions [54–56]. Current experiments are now able to prepare simple product states of excited spin spirals and tune the dimensionality and exchange interactions to probe the dynamics under different symmetries. Such experiments are now able to coherently evolve the system over unprecedentedly long timescales on the order of $t \sim 50\hbar/J$ [55] and, therefore, access the long-lived prethermal regime discussed in this work. On a different front, experiments in solid-state systems are now able to drive low-dimensional ferromagnetic and antiferromagnetic insulators and probe magnetization fluctuations with energy resolution using local probes [57–61], such as nitrogen-vacancy centers in diamond. Such experiments are capable of directly measuring the power-law distribution in Eq. (1) as well as the relaxation dynamics of highly excited states.

The outline of the paper is as follows: In Sec. II, we describe the Heisenberg model and the initial conditions. In Sec. III, we present a simple statistical mechanics model used to derive the scaling exponents analytically. In Sec. IV, we use phase-space methods to numerically evaluate the scaling exponents. In Sec. V, we discuss the connections between our work and previously studied instances of scaling in related models, and also present the conclusions. In the Appendixes we provide additional details about asymptotic functions used in Sec. III (Appendix A) and details about the statistical analysis used to analyze the numerical data (Appendix B).

II. MICROSCOPIC MODEL

We consider the Heisenberg antiferromagnet on a two-dimensional square lattice with linear size L, lattice constant ℓ, and with nearest-neighbor interactions:

$$H = J \sum_{\langle ij \rangle} S_i^x S_j^x + S_i^y S_j^y + S_i^z S_j^z. \tag{2}$$

Here $\boldsymbol{S}_i = (S_i^x, S_i^y, S_i^z)$ are spin S operators, $\langle ij \rangle$ denotes summation over nearest-neighbor spins i and j, and J is a positive constant. For the purposes of our work, including additional

next-nearest-neighbor exchange has no effect on the universal aspects of dynamics, so long as the next-nearest-neighbor exchange does not induce frustration. As such, we restrict our discussion to nearest-neighbor coupling only in order to keep the model as simple as possible. However, we emphasize that the SU(2) symmetry is essential to our discussion and breaking it will lead to qualitatively distinct exponents, as we discuss in more detail below.

As initial condition, we use an antiferromagnetic spin-spiral product state:

$$\langle S_i^{\pm}\rangle = S(-1)^{r_i^x+r_i^y}\sin\theta e^{\pm i\boldsymbol{q}\cdot\boldsymbol{r}_i},$$
$$\langle S_i^{z}\rangle = S(-1)^{r_i^x+r_i^y}\cos\theta, \tag{3}$$

where $S_i^{\pm} = S_i^x \pm S_i^y$. The initial condition (3) imprints a length scale $\xi = 2\pi/|\boldsymbol{q}|$ in which spins have Neel order (although there is no order globally) while restricting dynamics in the zero magnetization sector $S^{\rm tot} = 0$. Dynamics of spin systems under this type of initial conditions are now routinely accessed in cold-atomic platforms [54,55,62,63].

Insights about the nonequilibrium behavior of the Heisenberg antiferromagnet can be gained by first analyzing the low-energy properties of the system. At zero temperature, the two-dimensional Heisenberg antiferromagent on the square lattice exhibits a broken-symmetry ground state with a nonzero staggered magnetization (or Neel order). In this broken-symmetry state, the staggered magnetization $M^a = \sum_i (-1)^{r_i^x+r_i^y} S_i^a$ has finite expectation value, with $\boldsymbol{r}_i = (r_i^x, r_i^y)$ the lattice coordinate of spin i (expressed in units of lattice constant, thus, $r_i^{x,y}$ are integer numbers). Unlike the ferromagnetic case ($J < 0$), the antiferromagnetic ground state is not classical and has zero-point motion due to quantum fluctuations, i.e., $\langle M^a\rangle_{T=0} < NS$. Importantly, the broken-symmetry ground state persists for all values of S, even in the quantum limit $S = \frac{1}{2}$ [64,65].

For finite-energy states, the system does not exhibit long-range order. However, fluctuations of the staggered magnetization are relevant for finite energies as these have a quasi-long-range character, a feature coming from the system being at the critical dimension $d = 2$. As a result, it takes a parametrically long time for the system to erase the initial length scale ξ imprinted by the initial condition. In a loose sense, the "large-N" parameter governing the relaxation dynamics of the Heisenberg antiferromagnet is $S(\xi/\ell)^2$, which is roughly the total (staggered) magnetization of an island of radius ξ (this parameter also governs the energy density of the initial condition). For these reasons, we expect that the universal prethermal dynamics discussed in this work will be independent of the spin number S, so long as the condition $S(\xi/\ell)^2 \gg 1$ is met by the initial state (3).

III. ANALYTICAL DERIVATION OF THE NONEQUILIBRIUM SCALING EXPONENTS

A. Phenomenology

In this section, we construct a simple nonequilibrium statistical mechanics model that captures the universal aspects of prethermalization in Heisenberg antiferromagnet (2), namely, the asymptotic form of the function $f(x) \sim 1/x^{\nu}$ and the numerical values of (α, β) in Eq. (1). The essence of the approach follows closely that used in Refs. [50,66] and relies on exploiting the length-scale separation of spin modes introduced by the initial condition, i.e., $\ell \ll \xi \ll L$. The value of ξ is time dependent: it is initially imprinted by the initial conditions and, as time evolves, it defines the typical correlation length of staggered magnetization fluctuations. There are two types of excitations that need to be incorporated simultaneously into our description. First, the initial state will trigger spatial fluctuations of Neel order which govern the dynamics of the staggered magnetization at wave vectors $|\boldsymbol{k}| \lesssim 1/\xi$. Such fluctuations are large in two-dimensional systems. Second, large-wave-vector $1/\xi \lesssim |\boldsymbol{k}| \ll 1/\ell$ excitations will mediate the transfer of energy and magnetization towards UV degrees of freedom. Whereas the former is described with a classical continuum theory, the latter are described using a kinetic theory of magnons within the wave turbulence formalism. The key difference between our approach and the conventional approach at low temperature and thermal equilibrium, where one describes response function in terms of a dilute number of magnons, is that fluctuations of the staggered magnetization are large and need to be incorporated into the dynamics.

We proceed in two steps. For wave vectors $1/\xi \lesssim |\boldsymbol{k}| \ll 1/\ell$, we study the dynamics of magnetization fluctuations by assuming that the staggered magnetization is uniform in space: in a loose sense, magnons with wave vectors $1/\xi \lesssim |\boldsymbol{k}| \ll 1/\ell$ effectively see a uniform magnetization background within the typical timescale of magnon-magnon collisions. As such, in Sec. III B we pin the antiferromagnetic order parameter and derive the effective kinetic theory for magnons. Using the wave turbulence formalism, we derive the power-law exponent ν in Sec. III C. In Sec. III D, we study dynamics of the order parameter within a continuum theory and determine the relevant nonlinearities that govern the resulting spatial-temporal scaling of magnetization fluctuations for wave vectors $|\boldsymbol{k}| \lesssim 1/\xi$. From a simple scaling analysis that employs the equations of motion and spin conservation laws we derive the scaling exponents (α, β) that govern the growth of $\xi \sim t^{\beta}$.

B. Dynamics of short wavelengths

In the presence of a uniform staggered magnetization, it is convenient to write the spin operators in terms of bosonic operators. Here we employ the Dyson-Maleev transformation [67]. Because of the antiferromagnetic nature of the ground state, we use two flavors of bosons to describe spins in the A and B sublattices (see Fig. 1):

$$S_i^z = S - a_i^\dagger a_i, \tag{4a}$$
$$S_i^+ = \sqrt{2S}\left(a_i - \frac{1}{2S}a_i^\dagger a_i a_i\right), \tag{4b}$$
$$S_i^- = \sqrt{2S}a_i^\dagger, \tag{4c}$$
$$S_j^z = -S + b_j^\dagger b_j, \tag{4d}$$
$$S_j^+ = \sqrt{2S}\left(b_j - \frac{1}{2S}b_j^\dagger b_j b_j\right), \tag{4e}$$
$$S_j^- = \sqrt{2S}b_j^\dagger. \tag{4f}$$

Here $S_i^{\pm}$ denotes $S_i^{\pm} = S_i^x \pm iS_i^y$, a_i and b_j are bosonic annihilation operators, and we use i (j) to label sites in the A (B) sublattice. We note that the Dyson-Maleev transformation produces the correct spin commutation relations but violates the property $(S_i^-)^\dagger = S_i^+$. In this case, the spin Hamiltonian becomes non-Hermitian. In contrast, the Holstein-Primakoff transformation, another commonly used transformation for spin systems [68], retains Hermiticity but generates an infinite series of interaction vertices. In spite of the non-Hermiticity property, the Dyson-Maleev transformation has proven to be more convenient for studying spin-wave interaction in ferromagnets and antiferromagnets: it reproduces all the perturbative results obtained with the Holstein-Primakoff transformation in a much faster and compact way [67,69,70].

Inserting Eqs. (4a)–(4f) into Eq. (2) and separating terms order by order, we find $H = -NJS^2 + H_0 + H_{\rm int}$, with

$$H_0 = JS\sum_{\langle ij\rangle}(a_i^\dagger a_i + b_j^\dagger b_j + a_i b_j + b_j^\dagger a_i^\dagger), \tag{5a}$$

$$H_{\rm int} = -\frac{J}{2}\sum_{\langle ij\rangle}(a_i^\dagger a_i a_i b_j + a_i^\dagger b_j^\dagger b_j^\dagger b_j + 2a_i^\dagger a_i b_j^\dagger b_j). \tag{5b}$$

Note that interactions are $O(1/S)$ at small boson densities and vanish in the classical limit $S \to \infty$. Going into Fourier space and defining $a_{\boldsymbol{k}} = \frac{1}{\sqrt{N}}\sum_i e^{-i\boldsymbol{k}\cdot\boldsymbol{r}_i}a_i$, $b_{\boldsymbol{k}} = \frac{1}{\sqrt{N}}\sum_i e^{-i\boldsymbol{k}\cdot\boldsymbol{r}_j}b_j$, the quadratic component of the Hamiltonian is given by

$$H_0 = JzS\sum_{\boldsymbol{k}}(a_{\boldsymbol{k}}^\dagger a_{\boldsymbol{k}} + b_{\boldsymbol{k}}^\dagger b_{\boldsymbol{k}} + \gamma_{\boldsymbol{k}} a_{\boldsymbol{k}}^\dagger b_{-\boldsymbol{k}}^\dagger + \gamma_{\boldsymbol{k}} a_{\boldsymbol{k}} b_{-\boldsymbol{k}}). \tag{6}$$

Here $\gamma_{\boldsymbol{k}}$ denotes the phase factor $\gamma_{\boldsymbol{k}} = \frac{1}{z}\sum_{\boldsymbol{\ell}} e^{i\boldsymbol{k}\cdot\boldsymbol{\ell}}$, where $\boldsymbol{\ell}$ denotes the nearest-neighbor lattice vectors $\boldsymbol{\ell} = \{(\pm\ell, 0), (0, \pm\ell)\}$, and z is the coordination number of each spin ($z = 4$ in a two-dimensional square lattice). The quartic component of the Hamiltonian is given by

$$H_{\rm int} = -\frac{Jz}{2N}\sum_{\boldsymbol{k}_1\boldsymbol{k}_2\boldsymbol{k}_3\boldsymbol{k}_4}\delta(\boldsymbol{k}_{\rm i} - \boldsymbol{k}_{\rm f})(\gamma_{\boldsymbol{k}_4} a_{\boldsymbol{k}_1}^\dagger a_{-\boldsymbol{k}_2} a_{\boldsymbol{k}_3} b_{\boldsymbol{k}_4} + \gamma_{\boldsymbol{k}_1} a_{\boldsymbol{k}_1}^\dagger b_{\boldsymbol{k}_2}^\dagger b_{-\boldsymbol{k}_3}^\dagger b_{\boldsymbol{k}_4} + 2\gamma_{\boldsymbol{k}_3-\boldsymbol{k}_2} a_{\boldsymbol{k}_1}^\dagger b_{\boldsymbol{k}_2}^\dagger b_{\boldsymbol{k}_3} a_{\boldsymbol{k}_4}),$$

with $\boldsymbol{k}_{\rm i} = \boldsymbol{k}_1 + \boldsymbol{k}_2$ and $\boldsymbol{k}_{\rm f} = \boldsymbol{k}_3 + \boldsymbol{k}_4$.

We now proceed to diagonalize H_0 using the Bogoliubov transformation

$$a_{\boldsymbol{k}} = u_{\boldsymbol{k}}\alpha_{\boldsymbol{k}} - v_{\boldsymbol{k}}\beta_{-\boldsymbol{k}}^\dagger, \tag{7a}$$

$$b_{-\boldsymbol{k}}^\dagger = -v_{\boldsymbol{k}}\alpha_{\boldsymbol{k}} + u_{\boldsymbol{k}}\beta_{-\boldsymbol{k}}^\dagger, \tag{7b}$$

where $\alpha_{\boldsymbol{k}}$ and $\beta_{\boldsymbol{k}}$ are bosonic annihilation operators (bosonic commutation requires $u_{\boldsymbol{k}}^2 - v_{\boldsymbol{k}}^2 = 1$). Replacing Eq. (7) into (6) leads to

$$H_0 = \sum_{\boldsymbol{k}}\varepsilon_{\boldsymbol{k}}(\alpha_{\boldsymbol{k}}^\dagger\alpha_{\boldsymbol{k}} + \beta_{\boldsymbol{k}}^\dagger\beta_{\boldsymbol{k}}), \quad \varepsilon_{\boldsymbol{k}} = zJS\sqrt{1-\gamma_{\boldsymbol{k}}}, \tag{8}$$

and the factors $u_{\boldsymbol{k}}$ and $v_{\boldsymbol{k}}$ are given by

$$u_{\boldsymbol{k}} = \sqrt{\frac{1+\varepsilon_{\boldsymbol{k}}}{2\varepsilon_{\boldsymbol{k}}}}, \quad v_{\boldsymbol{k}} = \sqrt{\frac{1-\varepsilon_{\boldsymbol{k}}}{2\varepsilon_{\boldsymbol{k}}}}. \tag{9}$$

Using the Bogoliubov transformation on the quartic components of H results in

$$\begin{aligned} H_{\rm int} = -\frac{Jz}{2N}\sum_{\boldsymbol{k}_1\boldsymbol{k}_2\boldsymbol{k}_3\boldsymbol{k}_4}\delta(\boldsymbol{k}_{\rm i} - \boldsymbol{k}_{\rm f})u_{\boldsymbol{k}_1}u_{\boldsymbol{k}_2}u_{\boldsymbol{k}_3}u_{\boldsymbol{k}_4}\big(&\Phi^{(1)}_{\boldsymbol{k}_1\boldsymbol{k}_2\boldsymbol{k}_3\boldsymbol{k}_4}\alpha_{\boldsymbol{k}_1}^\dagger\alpha_{\boldsymbol{k}_2}^\dagger\alpha_{\boldsymbol{k}_3}\alpha_{\boldsymbol{k}_4} + 2\Phi^{(2)}_{\boldsymbol{k}_1\boldsymbol{k}_2\boldsymbol{k}_3\boldsymbol{k}_4}\alpha_{\boldsymbol{k}_1}^\dagger\beta_{-\boldsymbol{k}_2}\alpha_{\boldsymbol{k}_3}\alpha_{\boldsymbol{k}_4} + 2\Phi^{(3)}_{\boldsymbol{k}_1\boldsymbol{k}_2\boldsymbol{k}_3\boldsymbol{k}_4}\alpha_{\boldsymbol{k}_1}^\dagger\alpha_{\boldsymbol{k}_2}^\dagger\alpha_{\boldsymbol{k}_3}\beta_{-\boldsymbol{k}_4}^\dagger \\ &+ 4\Phi^{(4)}_{\boldsymbol{k}_1\boldsymbol{k}_2\boldsymbol{k}_3\boldsymbol{k}_4}\alpha_{\boldsymbol{k}_1}^\dagger\beta_{-\boldsymbol{k}_2}\alpha_{\boldsymbol{k}_3}\beta_{-\boldsymbol{k}_4}^\dagger + 2\Phi^{(5)}_{\boldsymbol{k}_1\boldsymbol{k}_2\boldsymbol{k}_3\boldsymbol{k}_4}\beta_{-\boldsymbol{k}_1}\beta_{-\boldsymbol{k}_2}\alpha_{\boldsymbol{k}_3}\beta_{-\boldsymbol{k}_4}^\dagger + 2\Phi^{(6)}_{\boldsymbol{k}_1\boldsymbol{k}_2\boldsymbol{k}_3\boldsymbol{k}_4}\alpha_{\boldsymbol{k}_1}^\dagger\beta_{-\boldsymbol{k}_2}\beta_{-\boldsymbol{k}_3}^\dagger\beta_{-\boldsymbol{k}_4}^\dagger + \Phi^{(7)}_{\boldsymbol{k}_1\boldsymbol{k}_2\boldsymbol{k}_3\boldsymbol{k}_4}\alpha_{\boldsymbol{k}_1}^\dagger\alpha_{\boldsymbol{k}_2}^\dagger\beta_{-\boldsymbol{k}_3}^\dagger\beta_{-\boldsymbol{k}_4}^\dagger \\ &+ \Phi^{(8)}_{\boldsymbol{k}_1\boldsymbol{k}_2\boldsymbol{k}_3\boldsymbol{k}_4}\beta_{-\boldsymbol{k}_1}\beta_{-\boldsymbol{k}_2}\alpha_{\boldsymbol{k}_3}\alpha_{\boldsymbol{k}_4} + \Phi^{(9)}_{\boldsymbol{k}_1\boldsymbol{k}_2\boldsymbol{k}_3\boldsymbol{k}_4}\beta_{-\boldsymbol{k}_1}\beta_{-\boldsymbol{k}_2}\beta_{-\boldsymbol{k}_3}^\dagger\beta_{-\boldsymbol{k}_4}^\dagger\big), \end{aligned} \tag{10}$$

where the phase factors $\Phi^{(n)}_{\boldsymbol{k}_1\boldsymbol{k}_2\boldsymbol{k}_3\boldsymbol{k}_4}$ are explicitly written in Appendix A.

We now analyze Eqs. (6) and (10) in the limit $k \ll 1/\ell$ in order to determine the power laws characterizing the quasiparticle dispersion and their interactions. From Eq. (6) one finds the well-known dispersion of small-momenta magnons given by $\varepsilon_{\boldsymbol{k}} \propto |\boldsymbol{k}|$. A second useful relation that results from the linearized analysis is the ratio between the amplitude of the staggered magnetization and the total magnetization. This relation can be obtained directly from the Bogoliubov eigenvectors $(u_{\boldsymbol{k}}, v_{\boldsymbol{k}})$ in Eq. (9). Focusing on the staggered and total magnetization produced by the $\alpha_{\boldsymbol{k}}$ mode, we find that the staggered magnetization scales as $m_{\boldsymbol{k}} \approx a_{\boldsymbol{k}} - b_{\boldsymbol{k}} \approx (u_{\boldsymbol{k}} + v_{\boldsymbol{k}})\alpha_{\boldsymbol{k}}$, whereas the total magnetization scales as $s_{\boldsymbol{k}} = (a_{\boldsymbol{k}} + b_{\boldsymbol{k}}) \approx (u_{\boldsymbol{k}} - v_{\boldsymbol{k}})\alpha_{\boldsymbol{k}}$. Using the small wave-vector expansion $|\boldsymbol{k}| \ll 1/\ell$ of Eq. (9), $u_{\boldsymbol{k}} \pm v_{\boldsymbol{k}} \approx \frac{1}{\sqrt{2\varepsilon_{\boldsymbol{k}}}}(1 \pm 1 + \frac{\varepsilon_{\boldsymbol{k}}\mp\varepsilon_{\boldsymbol{k}}}{2})$, combined with $\varepsilon_{\boldsymbol{k}} \propto |\boldsymbol{k}|$, we find $s_{\boldsymbol{k}} \approx |\boldsymbol{k}|m_{\boldsymbol{k}} \ll m_{\boldsymbol{k}}$, thus the total magnetization fluctuations are $O(|\boldsymbol{k}|\xi)$ smaller than the staggered magnetization fluctuations and vanish in the $|\boldsymbol{k}| \to 0$ limit, as expected for an antiferromagnet.

We now analyze the scaling of the interaction vertex $H_{\rm int}$ in Eq. (10) in the small wave-vector limit $|\boldsymbol{k}| \ll 1/\ell$. A detailed analysis of magnon relaxation in different energy ranges was done in Ref. [67]. Of primary interest in this work are on-shell processes describing particle-conserving collision between magnons. Off-resonant processes and processes which do not preserve particle number, both of which we will neglect, were shown to give subleading effects in the relaxation dynamics at small wave vectors $|\boldsymbol{k}| \ll 1/\ell$ [67]. Thus, the relevant terms in Eq. (10) are those containing the phase factors $\Phi^{(1)}$, $\Phi^{(4)}$, and $\Phi^{(9)}$, with $\Phi^{(1)} = \Phi^{(9)}$, which are associated to particle-conserving processes. For small wave vectors, the product $u_{\boldsymbol{k}_1}u_{\boldsymbol{k}_2}u_{\boldsymbol{k}_3}u_{\boldsymbol{k}_4}$ scales as $u_{\boldsymbol{k}_1}u_{\boldsymbol{k}_2}u_{\boldsymbol{k}_3}u_{\boldsymbol{k}_4} \sim \frac{1}{\sqrt{\varepsilon_{\boldsymbol{k}_1}\varepsilon_{\boldsymbol{k}_2}\varepsilon_{\boldsymbol{k}_3}\varepsilon_{\boldsymbol{k}_4}}} \sim 1/k^2$. In addition, the asymptotic form of $\Phi^{(1,9)}$ is given by $\Phi^{(1,9)}_{\boldsymbol{k}_1\boldsymbol{k}_2\boldsymbol{k}_3\boldsymbol{k}_4} =$

$2\varepsilon_{\boldsymbol{k}_3}\varepsilon_{\boldsymbol{k}_4}(\hat{\boldsymbol{k}}_3\cdot\hat{\boldsymbol{k}}_4-1)$ and the asymptotic form of $\Phi^{(4)}$ is given by $\Phi^{(4)}_{\boldsymbol{k}_1\boldsymbol{k}_2\boldsymbol{k}_3\boldsymbol{k}_4}=2\varepsilon_{\boldsymbol{k}_3}\varepsilon_{\boldsymbol{k}_4}(\hat{\boldsymbol{k}}_3\cdot\hat{\boldsymbol{k}}_4+1)$ (see Appendix A), and they all scale as $\Phi^{(n)}_{\boldsymbol{k}_1\boldsymbol{k}_2\boldsymbol{k}_3\boldsymbol{k}_4}\sim k^2$. As such, the matrix element for the two-body interaction $(\boldsymbol{k}_1,\boldsymbol{k}_2)\to(\boldsymbol{k}_3,\boldsymbol{k}_4)$ scales as $V(\lambda\boldsymbol{k}_1,\lambda\boldsymbol{k}_2,\lambda\boldsymbol{k}_3,\lambda\boldsymbol{k}_4)=\lambda^0V(\boldsymbol{k}_1,\boldsymbol{k}_2,\boldsymbol{k}_3,\boldsymbol{k}_4)$.

As a side remark, we note that if SU(2) symmetry is broken, for example by adding anisotropic exchange, then the scaling with momentum of the interactions changes altogether. In particular, the phase factors $\Phi^{(n)}_{\boldsymbol{k}_1\boldsymbol{k}_2\boldsymbol{k}_3\boldsymbol{k}_4}$ become wave-vector independent and this would change the dynamical scaling laws characterizing the prethermal regime. In contrast, adding next-nearest-neighbor exchange terms which preserve SU(2) symmetry will not alter the scaling behavior described below.

C. Scaling of the envelope function f

We now calculate the power-law scaling of the function $f(x)\sim 1/x^{\nu}$ using the wave turbulence formalism. Wave turbulence [2,3] provides a framework for computing the scaling of two-point correlation functions in far-from-equilibrium regimes when the system exhibits a weak coupling limit. In our case, the weak coupling limit is controlled by the parameter $\frac{1}{S}(\frac{\ell}{\xi})^2$. The starting point in wave turbulence theory is to assume incoherent dynamics of the bosonic degrees of freedom $\alpha_{\boldsymbol{k}}$ and $\beta_{\boldsymbol{k}}$, i.e., $\langle\alpha_{\boldsymbol{k}}\rangle=\langle\beta_{\boldsymbol{k}}\rangle=0$, which is equivalent to assuming that transverse magnetization fluctuations (relative to the direction of the Neel order) are incoherent. This approximation is only valid for excitations with wave vectors $1/\xi\lesssim|\boldsymbol{k}|\ll 1/\ell$. In the regime $|\boldsymbol{k}|\lesssim 1/\xi$, instead, there will be finite expectation value for $\langle\alpha_{\boldsymbol{k}}\rangle$ and $\langle\beta_{\boldsymbol{k}}\rangle$ signaling quasi-long-range order (this regime will be analyzed in the next section). Under this approximation, each flavor of magnons is characterized by its occupation number $\langle\alpha^{\dagger}_{\boldsymbol{k}}\alpha_{\boldsymbol{k}}\rangle=n_{\alpha,\boldsymbol{k}}$ and $\langle\beta^{\dagger}_{\boldsymbol{k}}\beta_{\boldsymbol{k}}\rangle=n_{\beta,\boldsymbol{k}}$. The standard procedure in wave turbulence consists of (i) deriving a kinetic equation from Eqs. (6) and (10) describing the time evolution of $n_{\boldsymbol{k}}$, (ii) proposing a solution of the form $n_{\boldsymbol{k}}\propto|k|^{-\nu}$, and (iii) finding ν that gives rise to a steady-state solution. Here we also assume that $n_{\boldsymbol{k},\alpha}=n_{\boldsymbol{k},\beta}=n_{\boldsymbol{k}}$.

Following the discussion in Sec. III B, we employ an effective theory describing magnon excitations that only includes on-shell terms which preserve both particle number and energy. The exponent ν can only depend on the power γ of the quasiparticle dispersion $\varepsilon_{\boldsymbol{k}}\propto|\boldsymbol{k}|^{\gamma}$, the power δ of the interaction $V(\lambda\boldsymbol{k}_1,\lambda\boldsymbol{k}_2,\lambda\boldsymbol{k}_3,\lambda\boldsymbol{k}_4)=\lambda^{\delta}V(\boldsymbol{k}_1,\boldsymbol{k}_2,\boldsymbol{k}_3,\boldsymbol{k}_4)$, and the system's dimension d. Based on the results of the previous section, we have $\gamma=2$ and $\delta=0$. As shown in Refs. [2,3], there are two nonthermal solutions with scaling exponents

$$\nu_N=d+\frac{2\delta-\gamma}{3},\qquad \nu_E=d+\frac{2\delta}{3}. \tag{11}$$

The solution with scaling exponent ν_N is associated to a flux of quasiparticles cascading towards small momenta (inverse cascade), whereas the solution with scaling exponent $\nu_E=2$ is associated to a flux of energy cascading towards large momenta (direct cascade). The wave-vector range where particle number is concentrated, $k_N=\frac{1}{N}\int\frac{d\boldsymbol{k}}{(2\pi)^2}|\boldsymbol{k}|n_{\boldsymbol{k}}$, is where the quasiparticle cascade occurs, whereas the wave-vector range where energy is concentrated, $k_E=\frac{1}{E}\int\frac{d\boldsymbol{k}}{(2\pi)^2}|\boldsymbol{k}|n_{\boldsymbol{k}}\varepsilon_{\boldsymbol{k}}$, is where the energy cascade occurs. Because $k_N<k_E$, the inverse cascade occurs at smaller wave vectors than the energy cascade. Using the values d,δ,γ specific to our system, we find $\nu_N=\frac{4}{3}$ and $\nu_E=2$.

Finally, we note that the scaling exponents ν_N and ν_E characterize the distribution of the occupation numbers $n_{\alpha,\boldsymbol{k}}$ and $n_{\beta,\boldsymbol{k}}$ of the bosonic degrees of freedom rather than the spin degrees of freedom. Thus, the last step in our calculation is to transform back from bosonic operators into spin operators. We note that the spin operators are related to $(\alpha_{\boldsymbol{k}},\beta_{\boldsymbol{k}})$ through a Bogoliubov transformation [see Eq. (7)]. As such, the scaling with momentum of the spin-spin correlation function $\langle M^a_{-\boldsymbol{k}}M^a_{\boldsymbol{k}}\rangle$ is given by $\langle M^a_{-\boldsymbol{k}}M^a_{\boldsymbol{k}}\rangle\sim n_{\boldsymbol{k}}/k\sim 1/k^{\nu_{N,E}+1}$, thus $\nu=\nu_{N,E}+1$.

We comment on the validity of the exponents ν_N and ν_E. In particular, we need to question the validity of using a kinetic theory involving only on-resonant and particle-conserving terms while neglecting all other processes. The validity of these approximations will be confirmed numerically in the next section. Reference [67] does a detailed analysis of all the terms in Eq. (10), and finds that on-resonant and particle-conserving processes dominate in the $k\to 0$ limit, whereas other processes become incrementally more relevant at larger wave vectors. Because the inverse particle cascade occurs at smaller wave vectors than the direct energy cascade, $k_N\ll k_E$, we expect that the scaling exponent ν_N is more robust to relaxation mechanisms such as particle-nonconserving and off-resonant processes than the scaling exponent ν_E. Indeed, in our numerics below we find that the scaling exponent of $f(x)\sim 1/x^{\nu}$ matches remarkably well with $\nu=\nu_N+1$ but we do not observe a second wave-vector range with exponent $\nu=\nu_E+1$, which is consistent with the picture presented in Ref. [67].

D. Spatiotemporal scaling exponents

In this section, we focus on the dynamics of magnetization fluctuations with wave vectors $|\boldsymbol{k}|\lesssim 1/\xi$. We use the microscopic equations of motion in the continuum limit and analyze the role of leading-order nonlinearities to phenomenologically predict the exponents α and β governing the growth of $\xi(t)$ in Eq. (1). We define two spin fields $\boldsymbol{a}=\langle\boldsymbol{S}_{i\in A}\rangle$ and $\boldsymbol{b}=\langle\boldsymbol{S}_{j\in B}\rangle$ that characterize the average orientation of the spin $\boldsymbol{S}$ in sublattice A and B, respectively. We also define the staggered magnetization $\boldsymbol{m}=\boldsymbol{a}-\boldsymbol{b}$ and the total magnetization $\boldsymbol{s}=\boldsymbol{a}+\boldsymbol{b}$. Assuming that the fields $\boldsymbol{a}$ and $\boldsymbol{b}$ vary smoothly in space, we can expand the microscopic equations of motion for spins $\partial_t\boldsymbol{S}_i=\sum_j\boldsymbol{S}_i\times\boldsymbol{S}_j$ to leading order in gradients:

$$\partial_t\boldsymbol{a}=\boldsymbol{a}\times(z\boldsymbol{b}+\nabla^2\boldsymbol{b}), \tag{12}$$

$$\partial_t\boldsymbol{b}=\boldsymbol{b}\times(z\boldsymbol{a}+\nabla^2\boldsymbol{a}), \tag{13}$$

where time is expressed in units of $1/J$, and we approximated the sum over neighboring spins with the Laplacian $\sum_{\boldsymbol{\ell}}\boldsymbol{b}_{\boldsymbol{x}+\boldsymbol{\ell}}\approx z\boldsymbol{b}_{\boldsymbol{x}}+\nabla^2\boldsymbol{b}_{\boldsymbol{x}}$ and $\sum_{\boldsymbol{\ell}}\boldsymbol{a}_{\boldsymbol{x}+\boldsymbol{\ell}}\approx z\boldsymbol{a}_{\boldsymbol{x}}+\nabla^2\boldsymbol{a}_{\boldsymbol{x}}$. In terms of $\boldsymbol{m}$ and $\boldsymbol{s}$, we find

$$\partial_t\boldsymbol{s}=\frac{1}{2}\boldsymbol{s}\times\nabla^2\boldsymbol{s}-\frac{1}{2}\boldsymbol{m}\times\nabla^2\boldsymbol{m}, \tag{14a}$$

$$\partial_t\boldsymbol{m}=\frac{z}{2}\boldsymbol{m}\times\boldsymbol{s}-\frac{1}{2}\boldsymbol{s}\times\nabla^2\boldsymbol{m}+\frac{1}{2}\boldsymbol{m}\times\nabla^2\boldsymbol{s}. \tag{14b}$$

To find the values of (α, β) in Eq. (1) we look at Eq. (14b) and balance the time derivative of $\boldsymbol{m}$ with the leading nonlinearity, which is given by the first term on the right-hand side:

$$\partial_t m^a_{\boldsymbol{k}} \approx \frac{z}{2}\epsilon_{abc}\sum_{\boldsymbol{p}} m^b_{\boldsymbol{p}-\boldsymbol{k}} s^c_{\boldsymbol{p}}, \tag{15}$$

with ϵ_{abc} the Levi-Civita symbol. The second approximation that we use is $s^a_{\boldsymbol{k}} \sim |\boldsymbol{k}| m^a_{\boldsymbol{k}}$, which is justified from the linearized analysis of spin waves discussed above which showed that the total magnetization is $O(k)$ smaller than the staggered magnetization. The third approximation that we use is assuming that all modes with wave vector $|\boldsymbol{k}| \lesssim 1/\xi$ are macroscopic and democratically occupied for all spin orientations. As such, if we identify $\xi \sim t^\beta$ in Eq. (1) and take $f \sim O(1)$ at small wave vectors, then $m^a_{\boldsymbol{k}}$ scales as $m^a_{\boldsymbol{k}} \sim \xi^{\alpha/2\beta}$ and $s^a_{\boldsymbol{k}}$ scales as $s^a_{\boldsymbol{k}} \sim \xi^{\alpha/2\beta-1}$. Using this scaling form in the left-hand side of Eq. (15), we find $\partial_t m^a_{\boldsymbol{k}} \sim \xi^{(\alpha-2)/2\beta}$, where we used $\dot{\xi} = \xi^{1-1/\beta}$. The right-hand side of Eq. (15), instead, gives $\sum_{\boldsymbol{k}} m^b_{\boldsymbol{p}-\boldsymbol{k}} s^c_{\boldsymbol{p}} \sim \xi^{\alpha/\beta-d-1}$, where we approximated $\sum_{\boldsymbol{k}} = A\int \frac{d^d\boldsymbol{k}}{(2\pi)^d} \propto \xi^{-d}$ and A is the total area of the system. Equating both sides of Eq. (15) such that they both yield the same temporal scaling for $\xi(t)$ results in

$$2(d+1)\beta = \alpha + 2. \tag{16}$$

The second relation between α and β comes from the conservation of spin length, $\frac{1}{4}\int d\boldsymbol{x}(\boldsymbol{m}+\boldsymbol{s})^2 + (\boldsymbol{m}-\boldsymbol{s})^2 =$ constant. Using the scaling $m^a_{\boldsymbol{k}} \sim \xi^{\alpha/2\beta}$ and neglecting the contribution of the total magnetization $|\boldsymbol{s}| \ll \boldsymbol{m}$, we find the second condition

$$\alpha = d\beta. \tag{17}$$

Combining Eq. (16) with (17) in $d = 2$ yields

$$\alpha = 1, \quad \beta = 1/2. \tag{18}$$

We note that a similar analysis in the ferromagnetic case resulted in quantitatively different exponents $\alpha = \frac{2}{3}$ and $\beta = \frac{1}{3}$ [50], indicating that the Heisenberg ferromagnet and antiferromagnet belong to different nonequilibrium universality classes. In particular, the analog of Eq. (16) in the ferromagnetic case is $2(d+2)\beta = \alpha + 2$. The key difference between the ferromagnetic and antiferromagnetic case is coming from the different dispersion of quasi-long-range modes (quadratic versus linear) and the different nature of the scaling field (conserved versus nonconserved).

IV. NUMERICAL SIMULATIONS THROUGH PHASE-SPACE METHODS

We compute the real-time dynamics of quantum spins using the truncated Wigner approximation (TWA) [71–74]. This method incorporates quantum fluctuations by adding quantum noise in the initial conditions and evolving the classical trajectories using the classical equations of motion for spins $\partial_t \boldsymbol{S}_i = J\sum_j \boldsymbol{S}_i \times \boldsymbol{S}_j$. To sample the initial conditions in Eq. (3), we use a Gaussian approximation for the Wigner function given by

$$W\left(S^\perp_i, S^z_i\right) = \frac{2}{\pi S} e^{\frac{-(S^\perp_i)^2}{S}} \delta\left(S^z_i - S\right), \tag{19}$$

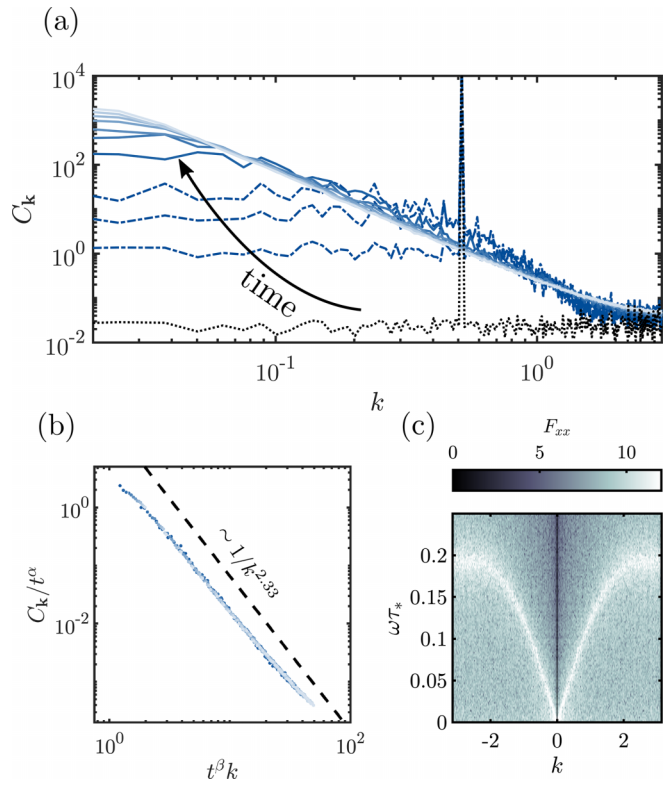

FIG. 2. (a) Evolution of the spin-spin correlation function for the staggered magnetization $C_{\boldsymbol{k}}(t) = \sum_a \langle M^a_{\boldsymbol{k}} M^a_{-\boldsymbol{k}}\rangle$. Shown with dotted lines is the correlation function for the initial state, with dashed-dotted lines is the correlation function prior to the self-similar regime, and with solid lines is the correlation function in the self-similar scaling regime. Lighter shade of color indicates increasing times. (b) Rescaled spin-spin correlation function using Eq. (1), with $\alpha = 1$ and $\beta = 0.5$. The dashed line indicates the power-law scaling $\sim x^{-7/3}$. (c) Unequal time spin-spin correlation function exhibiting a linearly dispersing gapless mode at small momenta. Simulation parameters: $L = 500$, $q_x = 0.5$, $\theta = \frac{\pi}{2}$, $S = 10$.

which reproduces the correct first and second moments of the Wigner distribution [71]. In Eq. (19), we assumed without loss of generality that the initial spin is pointing in the $+z$ direction.

Figure 2 shows the time evolution of the equal-time spin-spin correlation function for the staggered magnetization $C_{\boldsymbol{k}}(t) = \sum_{a=x,y,z}\langle M^a_{\boldsymbol{k}}(t) M^a_{-\boldsymbol{k}}(t)\rangle$ for a system of linear size $L = 500$, and initial conditions with wave vector $q_x = 0.5$, $q_y = 0$, and $\theta = \pi/2$. At $t = 0$, only a single mode with wave vector $\boldsymbol{k} = (q_x, 0)$ is macroscopically occupied. Within a timescale on the order of the inverse energy (per spin), the macroscopic state is depleted and a power-law distribution of the two-point correlation function develops. In this prethermal regime, we find that the values

$$\alpha = 1.0 \pm 0.1, \quad \beta = 0.48 \pm 0.05 \tag{20}$$

best fit the numerical data in a sufficiently long time window (see details in Appendix B). These values agree with the analytical predictions of the previous section using scaling arguments.

We now analyze the power-law scaling of the function f in Eq. (1) [see dashed lines in Fig. 2(b)]. Interestingly, we observe only *one* power law characterizing the tails of the magnetization fluctuation distribution, contrary to the predictions of wave turbulence found in Sec. III C which suggested the existence of two exponents ν_N and ν_E. In fitting the power-law exponent of the distribution we find that

$$\nu = 2.4 \pm 0.1, \tag{21}$$

which agrees with the exponent $\nu = \nu_N + 1 = \frac{7}{3} \approx 2.33$ associated to the inverse particle cascade. This result is in agreement with the conclusions of Ref. [67] which argues that off-resonant processes and particle nonconserving can be neglected at small momenta, thus the effective theory (6)–(10) considering only particle–conserving processes is a good approximation. For larger wave vectors (or energies), however, it is likely that off-resonant processes play a more prominent role and, therefore, the energy cascade exponent ν_E is not present.

We tested the robustness of our results using initial conditions with different values of θ, ranging from $\frac{\pi}{6} < \theta < \frac{\pi}{2}$ and different values of the wave vectors q_x, and we consistently see the same scaling exponents within numerical uncertainty. Similarly to the Heisenberg ferromagnet, this suggests that the far-from-equilibrium dynamics of the isotropic Heisenberg antiferromagnet is governed by a *single* nonthermal fixed point with the exponents in (20) and (21). This is unlike U(1) theories which exhibit multiple nonthermal fixed points, each of which can be activated by different initial conditions [48,53,75,76].

Whereas the ground state of the Heisenberg antiferromagnet exhibits gapless low-energy excitations, it is unclear whether the highly excited initial condition in Eq. (3) leads to a dynamically generated gap, such as those observed in O(n) and U(n) theories, or whether the spin modes in the self-similar region remain gapless. In a recent work [50], it was shown that the global SU(2) symmetry of the Heisenberg ferromagnet precludes the opening of a dynamical gap during evolution, leading to a long-lived prethermal regime governed by gapless modes with dispersion $\omega_{\boldsymbol{k}} \sim |\boldsymbol{k}|^2$. We numerically checked the nature of the excitations at the lowest wave vectors using the unequal-time correlation function $F_{xx}(\boldsymbol{k}, \omega) = \int dt\, e^{i\omega t} \langle \frac{1}{2}\{M^x_{-\boldsymbol{k}}(t_0 + t) M^x_{\boldsymbol{k}}(t_0)\}\rangle$ for the staggered magnetization ($\{A, B\} = AB + BA$) [see Fig. 2(c)]. Interestingly, we observe that the self-similar regime is governed by gapless modes at all times, even when the intermediate-time prethermal state is far from the ground state with uniform Neel order. The dispersion of the gapless mode is consistent with $\omega_{\boldsymbol{k}} \sim k$, different from the $\omega_{\boldsymbol{k}} \sim k^2$ dispersion observed in the Heisenberg ferromagnet.

V. DISCUSSION AND SUMMARY

The scaling regime discussed in this work is intrinsically different from previously studied instances of scaling in several important ways. Compared to the universal prethermal dynamics of Heisenberg ferromagnets [50], we find clearly distinct exponents originating from the existence of gapless modes with linear dispersion rather than modes with quadratic dispersion. In addition, unlike the ferromagnetic case, antiferromagnetic fluctuations are not coupled to any conserved charge. As a result, the long-lived prethermal regime discussed here is cut off by some parametrically long timescale controlled by nonuniversal processes that result in magnetization decay [e.g., particle-nonconserving terms in Eq. (10)].

Heisenberg antiferromagnets and O(n) theories share many similarities at thermodynamic equilibrium and low temperatures, such as linearly dispersing quasiparticles and a symmetry-breaking phase transition at $T = 0$ ($T > 0$) in dimension $d = 2$ ($d > 2$). We also find that they share some similarities in far-from-equilibrium regimes. For example, several works found similar scaling exponents as those we found above, $\alpha = d\beta$ and $\beta \approx \frac{1}{2}$, in O($n$) theories regardless of the value of n [48,53]. However, in O(n) theories quenched to (or across) a critical point [21,24,30] self-similarity occurs only if parameters and initial conditions are fine tuned so as to guarantee a vanishing late-time effective gap, unlike the antiferromagnetic case where we observe scaling without any fine tuning of the initial conditions. In addition, we observe quantitative differences in the universal scaling function f in Eq. (1) between both theories, reinforcing the idea that both models do not belong to the same nonequilibrium universality class.

Compared to nonthermal fixed points in bosonic U(1) theories, the key difference is that U(1) models can host topological defects (vortices) which can qualitatively alter the far-from-equilibrium behavior and give rise to different self-similar scaling regimes [75,76]. Even in the absence of vortices, the effective theory for the antiferromagnet differs from the U(1) bosonic theory both at the level of quasiparticle dispersion and their effective interactions, suggesting that both cannot belong to the same universality class. In certain cases, an effective gap has been observed to be dynamically generated by fluctuations [48,53]. This effective gap has been shown to lead to a modified nonrelativistic effective theory at low momenta and with scaling exponents $\alpha = d\beta$ and $\beta \approx \frac{1}{2}$, similar to those found in O(n) theories and Heisenberg antiferromagnets. However, at the level of the universal scaling function f in Eq. (1), we find a clearly distinct exponent ν which sets antiferromagnets and U(1) theories apart.

In summary, we studied the universal far-from-equilibrium dynamics of two-dimensional Heisenberg antiferromagnets. We showed that, if initialized in a state with inhomogeneous Neel order, magnetization fluctuations will exhibit a long-lived prethermal regime with universal behavior. Our results show that quantities which are neither conserved nor exhibit long-range order can still exhibit self-similiar behavior in a parametrically long time window. The scaling exponents are shown to be remarkably robust to details of the initial conditions: in particular, no fine tuning of the energy is necessary. Our work also highlights the important role played by dimensionality and symmetry in giving rise to gapless spin modes with quasi-long-range character. Combined with a recent work by one of us on Heisenberg ferromagnets [50], we have now fully characterized the nonthermal fixed points of the Heisenberg model both for ferromagnetic and antiferromagnetic exchanges. The scaling regime discussed in this work is readily accessible in ongoing experiments in cold-atomic gases which can probe these regimes in fully tunable

spin systems [55,77,78], including tunable symmetries and spatial dimension.

ACKNOWLEDGMENTS

We are grateful to J. Marino and A. Piñeiro-Orioli for insightful comments and previous collaborations. J.F.R.-N. acknowledges the Gordon and Betty Moore Foundation's EPiQS Initiative through Grants No. GBMF4302 and No. GBMF8686, the 2021 KITP program *Nonequilibrium universality: from classical to quantum and back*, and the National Science Foundation under Grant No. NSF PHY-1748958. P.G. is supported by the Alfred P. Sloan Foundation through Grant No. FG-2020-13615, the Department of Energy through Award No. DE-SC0019380, and the Simons Foundation through Award No. 620869.

APPENDIX A: INTERACTION COEFFICIENTS WITHIN THE DYSON-MALEEV FORMALISM

Here we reproduce the phase-factor coefficients of the interactions in the Heisenberg Hamiltonian [Eq. (10)] within the Dyson-Maleev transformation [Eq. (4a)] using the notation in Ref. [67]. In particular, the phase factors $\Phi^{(n)}$ appearing in the interactions of the effective Hamiltonian (10) are given by

$$\begin{aligned}\Phi^{(1,9)}_{k_1k_2k_3k_4} &= \big(\gamma_{k_1-k_4}x_{k_1}x_{k_4} + \gamma_{k_1-k_3}x_{k_1}x_{k_3} \\ &\quad + \gamma_{k_2-k_4}x_{k_2}x_{k_4} + \gamma_{k_2-k_3}x_{k_2}x_{k_3} - \gamma_{k_1}x_{k_2}x_{k_3}x_{k_4} \\ &\quad - \gamma_{k_2}x_{k_1}x_{k_3}x_{k_4} - \gamma_{k_2}x_{k_2} - \gamma_{k_1}x_{k_1}\big), \qquad \text{(A1a)}\\ \Phi^{(2,4)}_{k_1k_2k_3k_4} &= \big(-\gamma_{k_2-k_4}x_{k_4} - \gamma_{k_2-k_3}x_{k_3} \\ &\quad - \gamma_{k_1-k_4}x_{k_1}x_{k_2}x_{k_4} - \gamma_{k_1-k_3}x_{k_1}x_{k_2}x_{k_3} + \gamma_{k_1}x_{k_3}x_{k_4} \\ &\quad + \gamma_{k_2}x_{k_1}x_{k_2}x_{k_3}x_{k_4} + \gamma_{k_2} + \gamma_{k_1}x_{k_1}x_{k_2}\big), \qquad \text{(A1b)}\\ \Phi^{(3,5)}_{k_1k_2k_3k_4} &= \big(-\gamma_{k_2-k_4}x_{k_2} - \gamma_{k_1-k_4}x_{k_1} \\ &\quad - \gamma_{k_2-k_4}x_{k_1}x_{k_3}x_{k_4} - \gamma_{k_2-k_3}x_{k_2}x_{k_3}x_{k_4} + \gamma_{k_1}x_{k_2}x_{k_3} \\ &\quad + \gamma_{k_2}x_{k_1}x_{k_3} + \gamma_{k_2}x_{k_2}x_{k_4} + \gamma_{k_1}x_{k_1}x_{k_4}\big), \qquad \text{(A1c)}\\ \Phi^{(4)}_{k_1k_2k_3k_4} &= \big(\gamma_{k_2-k_4} + \gamma_{k_1-k_4}x_{k_1}x_{k_2} + \gamma_{k_1-k_4}x_{k_3}x_{k_4} \\ &\quad + \gamma_{k_1-k_3}x_{k_1}x_{k_2}x_{k_3}x_{k_4} - \gamma_{k_1}x_{k_3} - \gamma_{k_2}x_{k_1}x_{k_2}x_{k_3}\big) \\ &\quad - \gamma_{k_2}x_{k_4} - \gamma_{k_1}x_{k_1}x_{k_2}x_{k_4}, \qquad \text{(A1d)}\\ \Phi^{(7,8)}_{k_1k_2k_3k_4} &= \big(\gamma_{k_2-k_4}x_{k_2}x_{k_3} + \gamma_{k_2-k_3}x_{k_2}x_{k_4} \\ &\quad + \gamma_{k_2-k_3}x_{k_1}x_{k_3} + \gamma_{k_2-k_3}x_{k_1}x_{k_3} + \gamma_{k_2-k_4}x_{k_1}x_{k_4} \\ &\quad - \gamma_{k_1}x_{k_1}x_{k_3}x_{k_4} - \gamma_{k_2}x_{k_2}x_{k_3}x_{k_4} - \gamma_{k_1}x_{k_2} - \gamma_{k_2}x_{k_1}\big). \qquad \text{(A1e)}\end{aligned}$$

In these expressions, the parameter γ_k is given by $\gamma_k = \frac{1}{z}\sum_\ell e^{ik\cdot\ell}$ defined in the main text, where ℓ is the nearest-neighbor lattice vector in two dimensions. The parameter x_k is the ratio $x_k = u_k/v_k = \sqrt{(1-\varepsilon_k)/(1+\varepsilon_k)}$, with $\varepsilon_k = \sqrt{1-\gamma_k^2}$.

Of primary interest are the expressions in Eq. (A1) in the long-wavelength limit $|\boldsymbol{k}| \to 0$, particularly for the factors $\Phi^{(1)} = \Phi^{(9)}$, and $\Phi^{(4)}$ which contribute to particle-conserving scattering processes in the kinetic theory. We first note the following identities which hold in the asymptotic limit $|\boldsymbol{k}| \to 0$:

$$\begin{aligned}\varepsilon_k &\approx \tfrac{1}{2}|\boldsymbol{k}|, \qquad \text{(A2a)}\\ \gamma_k &\approx 1 - \tfrac{1}{2}\varepsilon_k^2, \qquad \text{(A2b)}\\ x_k &\approx 1 - \varepsilon_k. \qquad \text{(A2c)}\end{aligned}$$

Replacing these asymptotic expressions into Eq. (A1) and taking $\boldsymbol{k}_1 + \boldsymbol{k}_2 = \boldsymbol{k}_3 + \boldsymbol{k}_4$ due to momentum conservation leads to

$$\begin{aligned}\Phi^{(1,9)}_{k_1k_2k_3k_4} &= \tfrac{1}{2}\boldsymbol{k}_3\cdot\boldsymbol{k}_4 - 2\varepsilon_{k_3}\varepsilon_{k_4}, \qquad \text{(A3a)}\\ \Phi^{(4)}_{k_1k_2k_3k_4} &= \tfrac{1}{2}\boldsymbol{k}_3\cdot\boldsymbol{k}_4 + 2\varepsilon_{k_3}\varepsilon_{k_4}, \qquad \text{(A3b)}\end{aligned}$$

to leading order in momentum $\boldsymbol{k}$. These relations can also be written as

$$\begin{aligned}\tfrac{1}{2}\Phi^{(1,9)}_{k_1k_2k_3k_4} &= \varepsilon_{k_3}\varepsilon_{k_4}(\hat{k}_3\cdot\hat{k}_4 - 1),\\ \tfrac{1}{2}\Phi^{(4)}_{k_1k_2k_3k_4} &= \varepsilon_{k_3}\varepsilon_{k_4}(\hat{k}_3\cdot\hat{k}_4 + 1). \qquad \text{(A4a)}\end{aligned}$$

Importantly, these phase factors accounting for particle-conserving processes scale as $\Phi \sim \boldsymbol{k}^2$, which is used in the derivation of ν in Eq. (21) of the main text.

APPENDIX B: STATISTICAL ANALYSIS OF NUMERICAL DATA

We obtain the scaling exponents α and β that best fit the numerical data by minimizing the error function $E(\alpha,\beta)$ that quantifies the collapse of the data points through the scaling in Eq. (1). First, we take discrete values of $|\boldsymbol{k}| = k_i$ compatible with the inverse lattice spacing and evaluate the distribution $C(k,t_m)$ at different time steps t_m within the self-similar regime ($t_{m+1} - t_m \sim \tau$ is roughly the inverse energy of the system). Second, we define the rescaled variables $y_{i,m} = t_m^\alpha C(k_i,t_m)$ and $x_{i,m} = t_m^\beta k_i$. By interpolating these variables, we are able to obtain an explicit function $y_m(x)$, where x is assumed to be a continuum variable. Third, we compute the error function as

$$E(\alpha,\beta) = \sum_{m,m'}\int dx|y_m(x) - y_{m'}(x)|. \qquad \text{(B1)}$$

The contour plot of $E(\alpha,\beta)$ for the self-similar regime studied in Fig. 2 is shown in Fig. 3. We find that the best fitting with

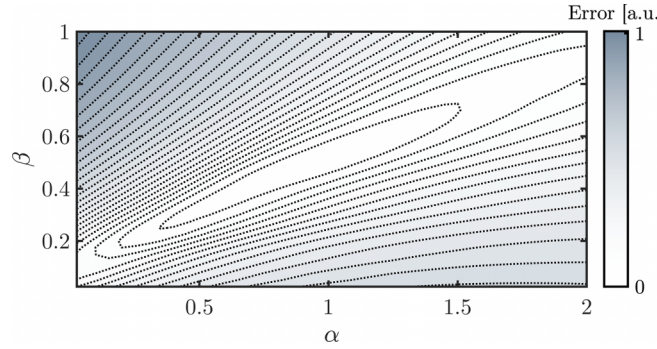

FIG. 3. Error function in Eq. (B1) plotted as a function of the fitting parameters α and β. Darker color indicates higher error values. The minimum of E occurs at around $\beta \approx 0.5$ and alpha $\alpha \approx 1$.

minimum error is centered around the point $(\alpha, \beta) \approx (1, 0.5)$, which is consistent with our theoretical prediction. The error bars are obtained from the sensitivity of the parameter (α, β) for different initial conditions.

[1] K. R. Sreenivasan, Fluid turbulence, Rev. Mod. Phys. **71**, S383 (1999).

[2] V. Zakharov, V. L'vov, V. L'vov, and G. Falkovich, *Kolmogorov Spectra of Turbulence I: Wave Turbulence* (Springer, Berlin, 1992).

[3] S. Nazarenko, *Wave Turbulence*, Lecture Notes in Physics (Springer, Berlin, 2011).

[4] P. Calabrese and A. Gambassi, Ageing properties of critical systems, J. Phys. A: Math. Gen. **38**, R133 (2005).

[5] A. Bray, Theory of phase-ordering kinetics, Adv. Phys. **43**, 357 (1994).

[6] M. Kardar, G. Parisi, and Y.-C. Zhang, Dynamic scaling of growing interfaces, Phys. Rev. Lett. **56**, 889 (1986).

[7] D. Forster, D. R. Nelson, and M. J. Stephen, Large-distance and long-time properties of a randomly stirred fluid, Phys. Rev. A **16**, 732 (1977).

[8] U. C. Täuber, *Critical Dynamics: A Field Theory Approach to Equilibrium and Non-equilibrium Scaling Behavior* (Cambridge University Press, Cambridge, 2014).

[9] L. M. Sieberer, A. Chiocchetta, A. Gambassi, U. C. Täuber, and S. Diehl, Thermodynamic equilibrium as a symmetry of the Schwinger-Keldysh action, Phys. Rev. B **92**, 134307 (2015).

[10] M. Crossley, P. Glorioso, and H. Liu, Effective field theory of dissipative fluids, J. High Energy Phys. 09 (2017) 095.

[11] C. Aron, G. Biroli, and L. F. Cugliandolo, (Non) equilibrium dynamics: a (broken) symmetry of the Keldysh generating functional, SciPost Phys. **4**, 008 (2018).

[12] A. Mitra, S. Takei, Y. B. Kim, and A. J. Millis, Nonequilibrium quantum criticality in open electronic systems, Phys. Rev. Lett. **97**, 236808 (2006).

[13] E. G. Dalla Torre, E. Demler, T. Giamarchi, and E. Altman, Dynamics and universality in noise-driven dissipative systems, Phys. Rev. B **85**, 184302 (2012).

[14] L. M. Sieberer, S. D. Huber, E. Altman, and S. Diehl, Dynamical critical phenomena in driven-dissipative systems, Phys. Rev. Lett. **110**, 195301 (2013).

[15] J. Marino and S. Diehl, Quantum dynamical field theory for nonequilibrium phase transitions in driven open systems, Phys. Rev. B **94**, 085150 (2016).

[16] A. Chiocchetta, A. Gambassi, S. Diehl, and J. Marino, Universal short-time dynamics: Boundary functional renormalization group for a temperature quench, Phys. Rev. B **94**, 174301 (2016).

[17] G. Aarts and J. Berges, Classical aspects of quantum fields far from equilibrium, Phys. Rev. Lett. **88**, 041603 (2002).

[18] J. Berges, S. Borsányi, and C. Wetterich, Prethermalization, Phys. Rev. Lett. **93**, 142002 (2004).

[19] J. Berges, A. Rothkopf, and J. Schmidt, Nonthermal fixed points: Effective weak coupling for strongly correlated systems far from equilibrium, Phys. Rev. Lett. **101**, 041603 (2008).

[20] J. Berges and D. Sexty, Strong versus weak wave-turbulence in relativistic field theory, Phys. Rev. D **83**, 085004 (2011).

[21] A. Chandran, A. Nanduri, S. S. Gubser, and S. L. Sondhi, Equilibration and coarsening in the quantum $O(N)$ model at infinite N, Phys. Rev. B **88**, 024306 (2013).

[22] J. Berges, K. Boguslavski, S. Schlichting, and R. Venugopalan, Turbulent thermalization process in heavy-ion collisions at ultrarelativistic energies, Phys. Rev. D **89**, 074011 (2014).

[23] J. Berges, K. Boguslavski, S. Schlichting, and R. Venugopalan, Universality far from equilibrium: From superfluid bose gases to heavy-ion collisions, Phys. Rev. Lett. **114**, 061601 (2015).

[24] A. Maraga, A. Chiocchetta, A. Mitra, and A. Gambassi, Aging and coarsening in isolated quantum systems after a quench: Exact results for the quantum O(n) model with $n \to \infty$, Phys. Rev. E **92**, 042151 (2015).

[25] A. Chiocchetta, M. Tavora, A. Gambassi, and A. Mitra, Short-time universal scaling and light-cone dynamics after a quench in an isolated quantum system in d spatial dimensions, Phys. Rev. B **94**, 134311 (2016).

[26] J. Berges, Nonequilibrium quantum fields: From cold atoms to cosmology, arXiv:1503.02907.

[27] K. Fujimoto and M. Tsubota, Direct and inverse cascades of spin-wave turbulence in spin-1 ferromagnetic spinor bose-einstein condensates, Phys. Rev. A **93**, 033620 (2016).

[28] J. Berges and B. Wallisch, Nonthermal fixed points in quantum field theory beyond the weak-coupling limit, Phys. Rev. D **95**, 036016 (2017).

[29] C.-M. Schmied, A. N. Mikheev, and T. Gasenzer, Prescaling in a far-from-equilibrium bose gas, Phys. Rev. Lett. **122**, 170404 (2019).

[30] A. Chiocchetta, A. Gambassi, S. Diehl, and J. Marino, Dynamical crossovers in prethermal critical states, Phys. Rev. Lett. **118**, 135701 (2017).

[31] N. Navon, A. L. Gaunt, R. P. Smith, and Z. Hadzibabic, Emergence of a turbulent cascade in a quantum gas, Nature (London) **539**, 72 (2016).

[32] C. Eigen, J. A. P. Glidden, R. Lopes, E. A. Cornell, R. P. Smith, and Z. Hadzibabic, Universal prethermal dynamics of bose gases quenched to unitarity, Nature (London) **563**, 221 (2018).

[33] S. Erne, R. Bücker, T. Gasenzer, J. Berges, and J. Schmiedmayer, Universal dynamics in an isolated one-dimensional bose gas far from equilibrium, Nature (London) **563**, 225 (2018).

[34] M. Prüfer, P. Kunkel, H. Strobel, S. Lannig, D. Linnemann, C.-M. Schmied, J. Berges, T. Gasenzer, and M. K. Oberthaler, Observation of universal dynamics in a spinor bose gas far from equilibrium, Nature (London) **563**, 217 (2018).

[35] J. A. P. Glidden, C. Eigen, L. H. Dogra, T. A. Hilker, R. P. Smith, and Z. Hadzibabic, Bidirectional dynamic scaling in an isolated Bose gas far from equilibrium, Nat. Phys. **17**, 457 (2021).

[36] B. Bertini, F. H. L. Essler, S. Groha, and N. J. Robinson, Prethermalization and thermalization in models with weak integrability breaking, Phys. Rev. Lett. **115**, 180601 (2015).

[37] V. B. Bulchandani, R. Vasseur, C. Karrasch, and J. E. Moore, Bethe-Boltzmann hydrodynamics and spin transport in the XXZ chain, Phys. Rev. B **97**, 045407 (2018).

[38] J. De Nardis, S. Gopalakrishnan, E. Ilievski, and R. Vasseur, Superdiffusion from emergent classical solitons in quantum spin chains, Phys. Rev. Lett. **125**, 070601 (2020).

[39] S. Gopalakrishnan and R. Vasseur, Kinetic theory of spin diffusion and superdiffusion in XXZ spin chains, Phys. Rev. Lett. **122**, 127202 (2019).

[40] A. Das, K. Damle, A. Dhar, D. A. Huse, M. Kulkarni, C. B. Mendl, and H. Spohn, Nonlinear fluctuating hydrodynamics for the classical xxz spin chain, J. Stat. Phys. **180**, 238 (2020).

[41] L. V. Delacrétaz and P. Glorioso, Breakdown of diffusion on chiral edges, Phys. Rev. Lett. **124**, 236802 (2020).

[42] P. Glorioso, J. Guo, J. F. Rodriguez-Nieva, and A. Lucas, Breakdown of hydrodynamics below four dimensions in a fracton fluid, Nat. Phys. **18**, 912 (2022).

[43] A. D. Rutenberg, Scaling violations with textures in two-dimensional phase ordering, Phys. Rev. E **51**, R2715 (1995).

[44] A. D. Rutenberg and A. J. Bray, Energy-scaling approach to phase-ordering growth laws, Phys. Rev. E **51**, 5499 (1995).

[45] P. Gagel, P. P. Orth, and J. Schmalian, Universal postquench prethermalization at a quantum critical point, Phys. Rev. Lett. **113**, 220401 (2014).

[46] P. Gagel, P. P. Orth, and J. Schmalian, Universal postquench coarsening and aging at a quantum critical point, Phys. Rev. B **92**, 115121 (2015).

[47] B. Sciolla and G. Biroli, Quantum quenches, dynamical transitions, and off-equilibrium quantum criticality, Phys. Rev. B **88**, 201110(R) (2013).

[48] K. Boguslavski and A. Piñeiro Orioli, Unraveling the nature of universal dynamics in $O(N)$ theories, Phys. Rev. D **101**, 091902(R) (2020).

[49] S. Bhattacharyya, J. F. Rodriguez-Nieva, and E. Demler, Universal prethermal dynamics in Heisenberg ferromagnets, Phys. Rev. Lett. **125**, 230601 (2020).

[50] J. F. Rodriguez-Nieva, A. P. Orioli, and J. Marino, Far-from-equilibrium universality in the two-dimensional heisenberg model, Proc. Natl. Acad. Sci. USA **119**, e2122599119 (2022).

[51] P. C. Hohenberg and B. I. Halperin, Theory of dynamic critical phenomena, Rev. Mod. Phys. **49**, 435 (1977).

[52] S. Sachdev, *Quantum Phase Transitions*, 2nd ed. (Cambridge University Press, Cambridge, 2011).

[53] A. Piñeiro Orioli, K. Boguslavski, and J. Berges, Universal self-similar dynamics of relativistic and nonrelativistic field theories near nonthermal fixed points, Phys. Rev. D **92**, 025041 (2015).

[54] S. Hild, T. Fukuhara, P. Schauß, J. Zeiher, M. Knap, E. Demler, I. Bloch, and C. Gross, Far-from-equilibrium spin transport in Heisenberg quantum magnets, Phys. Rev. Lett. **113**, 147205 (2014).

[55] P. N. Jepsen, J. Amato-Grill, I. Dimitrova, W. W. Ho, E. Demler, and W. Ketterle, Spin transport in a tunable Heisenberg model realized with ultracold atoms, Nature (London) **588**, 403 (2020).

[56] P. N. Jepsen, W. W. Ho, J. Amato-Grill, I. Dimitrova, E. Demler, and W. Ketterle, Transverse spin dynamics in the anisotropic Heisenberg model realized with ultracold atoms, Phys. Rev. X **11**, 041054 (2021).

[57] C. Du, T. van der Sar, T. X. Zhou, P. Upadhyaya, F. Casola, H. Zhang, M. C. Onbasli, C. A. Ross, R. L. Walsworth, Y. Tserkovnyak, and A. Yacoby, Control and local measurement of the spin chemical potential in a magnetic insulator, Science **357**, 195 (2017).

[58] J. F. Rodriguez-Nieva, D. Podolsky, and E. Demler, Probing hydrodynamic sound modes in magnon fluids using spin magnetometers, Phys. Rev. B **105**, 174412 (2022).

[59] T. X. Zhou, J. J. Carmiggelt, L. M. Gächter, I. Esterlis, D. Sels, R. J. Stöhr, C. Du, D. Fernandez, J. F. Rodriguez-Nieva, F. Büttner, E. Demler, and A. Yacoby, A magnon scattering platform, Proc. Natl. Acad. Sci. USA **118**, e2019473118 (2021).

[60] E. Lee-Wong, J. Ding, X. Wang, C. Liu, N. J. McLaughlin, H. Wang, M. Wu, and C. R. Du, Quantum sensing of spin fluctuations of magnetic insulator films with perpendicular anisotropy, Phys. Rev. Appl. **15**, 034031 (2021).

[61] H. Wang, Y. Xiao, M. Guo, E. Lee-Wong, G. Q. Yan, R. Cheng, and C. R. Du, Spin pumping of an easy-plane antiferromagnet enhanced by Dzyaloshinskii–Moriya interaction, Phys. Rev. Lett. **127**, 117202 (2021).

[62] M. Babadi, E. Demler, and M. Knap, Far-from-equilibrium field theory of many-body quantum spin systems: Prethermalization and relaxation of spin spiral states in three dimensions, Phys. Rev. X **5**, 041005 (2015).

[63] J. F. Rodriguez-Nieva, A. Schuckert, D. Sels, M. Knap, and E. Demler, Transverse instability and universal decay of spin spiral order in the heisenberg model, Phys. Rev. B **105**, L060302 (2022).

[64] D. A. Huse and V. Elser, Simple variational wave functions for two-dimensional Heisenberg spin-$\frac{1}{2}$ antiferromagnets, Phys. Rev. Lett. **60**, 2531 (1988).

[65] J. D. Reger and A. P. Young, Monte carlo simulations of the spin-(1/2 heisenberg antiferromagnet on a square lattice, Phys. Rev. B **37**, 5978 (1988).

[66] J. F. Rodriguez-Nieva, Turbulent relaxation after a quench in the heisenberg model, Phys. Rev. B **104**, L060302 (2021).

[67] A. B. Harris, D. Kumar, B. I. Halperin, and P. C. Hohenberg, Dynamics of an antiferromagnet at low temperatures: Spin-wave damping and hydrodynamics, Phys. Rev. B **3**, 961 (1971).

[68] T. Holstein and H. Primakoff, Field dependence of the intrinsic domain magnetization of a ferromagnet, Phys. Rev. **58**, 1098 (1940).

[69] C. M. Canali, S. M. Girvin, and M. Wallin, Spin-wave velocity renormalization in the two-dimensional Heisenberg antiferromagnet at zero temperature, Phys. Rev. B **45**, 10131 (1992).

[70] C. J. Hamer, Z. Weihong, and P. Arndt, Third-order spin-wave theory for the heisenberg antiferromagnet, Phys. Rev. B **46**, 6276 (1992).

[71] A. Polkovnikov, Phase space representation of quantum dynamics, Ann. Phys. **325**, 1790 (2010).

[72] S. M. Davidson and A. Polkovnikov, $SU(3)$ semiclassical representation of quantum dynamics of interacting spins, Phys. Rev. Lett. **114**, 045701 (2015).

[73] J. Schachenmayer, A. Pikovski, and A. M. Rey, Many-body quantum spin dynamics with Monte Carlo trajectories on a discrete phase space, Phys. Rev. X **5**, 011022 (2015).

[74] B. Zhu, A. M. Rey, and J. Schachenmayer, A generalized phase space approach for solving quantum spin dynamics, New J. Phys. **21**, 082001 (2019).

[75] B. Nowak, D. Sexty, and T. Gasenzer, Superfluid turbulence: Nonthermal fixed point in an ultracold bose gas, Phys. Rev. B **84**, 020506(R) (2011).

[76] B. Nowak, J. Schole, D. Sexty, and T. Gasenzer, Nonthermal fixed points, vortex statistics, and superfluid turbulence in an ultracold bose gas, Phys. Rev. A **85**, 043627 (2012).

[77] L.-M. Duan, E. Demler, and M. D. Lukin, Controlling spin exchange interactions of ultracold atoms in optical lattices, Phys. Rev. Lett. **91**, 090402 (2003).

[78] E. J. Davis, G. Bentsen, L. Homeier, T. Li, and M. H. Schleier-Smith, Photon-mediated spin-exchange dynamics of spin-1 atoms, Phys. Rev. Lett. **122**, 010405 (2019).